INTERNATIONAL JOURNAL OF HYDROGEN ENERGY XXX (2015) 1–8

Available online at www.sciencedirect.com

ScienceDirect

journal homepage: www.elsevier.com/locate/he

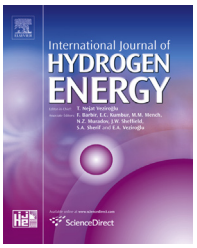

Controllable lithium storage performance of tin oxide anodes with various particle sizes

Haoze Song [a], *Xifei Li* [a,*], *Yanhua Cui* [b], *Dongbin Xiong* [a], *Yufen Wang* [a], *Jiesheng Zeng* [a], *Litian Dong* [a], *Dejun Li* [a,*], *Xueliang Sun* [c,a]

[a] *Energy & Materials Engineering Centre, College of Physics and Materials Science, Tianjin Normal University, Tianjin 300387, China*

[b] *Institute of Electronic Engineering, CAEP, Mianyang 621900, China*

[c] *Nanomaterials and Energy Lab, Department of Mechanical and Materials Engineering, Western University, London, Ontario N6A 5B9, Canada*

ARTICLE INFO

Article history:
Received 17 December 2014
Received in revised form
3 March 2015
Accepted 17 March 2015
Available online xxx

Keywords:
Lithium ion batteries
Anode material
SnO_2
Nanoparticle size
Electrochemical performance

ABSTRACT

The SnO_2 anode materials with various nanoparticle sizes were successfully synthesized to study their size effects on lithium storage performance. The compositions, structures, particle sizes and morphologies of the as-prepared samples were characterized by X-ray diffraction (XRD), Raman spectra, X-ray photoelectron spectroscopy (XPS), Scanning electron microscope (SEM) and high resolution transmission electron microscopy (HRTEM) techniques. It was confirmed that the obtained nanomaterials via a facile reflux approach show smaller size than that of hydrothermal method. Using cyclic voltammograms, electrochemical impedance spectroscopy, and galvanostatical charge/discharge testing, the SnO_2 anodes with different nanoparticle sizes exhibit various electrochemical performance with lithium, originating from the enormous volume changes associated with the alloying and de-alloying processes. It was demonstrated that the anode material with smaller nanoparticle size performs much better lithium storage performance.

Introduction

The increased lack of energy and the severe changes in the earth's ecological environment have gradually been proven to be two obstacles hindering the development of the human civilization. With the huge consumption of fossil fuels and the drying up of resources, the greenhouse effect and air pollution has posed a serious threat on earth environment. The research and development of low or free pollution energy storage and conversion has become the urgent challenges. Among various energy storage and conversion, a lithium ion battery, as an ideal energy system in the 21st century, arouses the attractive attention in the world.

In a commercial lithium ion battery, graphite anode better solves the battery stability problem. However, the graphite anode itself does not overcome an obvious disadvantage of low specific capacity of 372 mAh g^{-1} corresponding to Li_6C [1]. To address this problem, many researchers have been pursuing some potential carbon-free anodes with high specific

* *Corresponding authors*. Tel.: +86 22 23766526; fax: +86 22 23766503.
E-mail addresses: xfli2011@hotmail.com (X. Li), dejunli@mail.tjnu.edu.cn (D. Li).

http://dx.doi.org/10.1016/j.ijhydene.2015.03.168
0360-3199/

capacities, such as Si, Sn, and SnO_2, etc. In comparison to commercial graphite, the SnO_2 anode shows obvious advantages of low cost and high reversible discharge capacity (782 mAh g^{-1}) attracting much attention [2]. In one mol SnO_2 anode, up to 4.4 mol Li-ions can be stored ($Li_{22}Sn_5$) with increased energy capacity [3,4], which results in huge volume change of around 259% occurred upon cycling [5–8]. As a result, some cracks occur in the SnO_2 anode, accompanied by an electrical contact loss of active material with the current collectors and/or the conductive agent, thereby causing the poor cycling performance [9].

It was reported that to reduce the particle size of SnO_2 will increase the surface to volume ratio, and decrease the absolute volume changes during lithium insertion and extraction [10]. For example, Kim et al. employed the hydrothermal method to obtain SnO_2 ultrafine nanoparticles with size of 3 nm, 4 nm, and 8 nm. They reported that SnO_2 particles with 3 nm size showed the best electrochemical performance among three anode materials. However, the obtained anodes were with very similar size less than 10 nm, which showed some limitation to highlight the effects of SnO_2 particle size on lithium storage performance. Moreover, the synthesis approach they used exhibits some possible difficulties in scale-up.

In this study, the SnO_2 anodes with different particle sizes (say 15 nm, 30 nm, and 70 nm) were successfully obtained, moreover, the particle size effects of SnO_2 anodes on battery performance were studied in detail. It is expected that the SnO_2 nanoparticles with smaller size could well buffer volume change of the anodes upon cycles, and result in better electrochemical performance.

Experimental

Synthesis of SnO_2 nanoparticles

Nanocrystalline SnO_2–I was synthesized by a facile reflux method as follows: (1) 2.256 g of $SnCl_2 \cdot 2H_2O$ (98%, Aladdin) was dissolved in 50 mL ethanol (Tianjin Jiangtian Chemical Co. Ltd), which was stirred for 30 min. (2) 50 mL distilled water was added into the 150 ml of three flask. (3) Solution (1) was mixed with Solution (2) drop by drop, and stirred at 100 °C for 12 h with the reflux. The resultant gel was cleaned by deionized water and ethanol for three times in a centrifuge, respectively. The final product was dried at 80 °C for 12 h, and calcined at 500 °C for 3 h in a muffle furnace.

SnO_2-II was synthesized via a hydrothermal method, and the process was similar to that of SnO_2–I. The difference is that after Solution (1) was mixed with Solution (2) drop by drop, the mixture solution was transferred to a 50 mL Teflon-lined autoclave. The reaction was still maintained at 100 °C for 12 h in a Teflon-lined autoclave. The post-treatment is the same as SnO_2–I.

For comparison, the commercial SnO_2 nanoparticles with a size of 70 nm were purchased from Aladdin, marked as SnO_2-III.

The microstructure of the as-prepared SnO_2 was characterized by X-ray diffraction (XRD), Raman spectroscopy (LabRAM HR800), and X-ray photoelectron spectroscopy (Bruker D8). The obtained morphology was examined by scanning electron microscopy (SEM) which was performed on a Hitachi SU8010 and high resolution transmission electron microscopy (HRTEM) conducted on JEOL JEM-3000F.

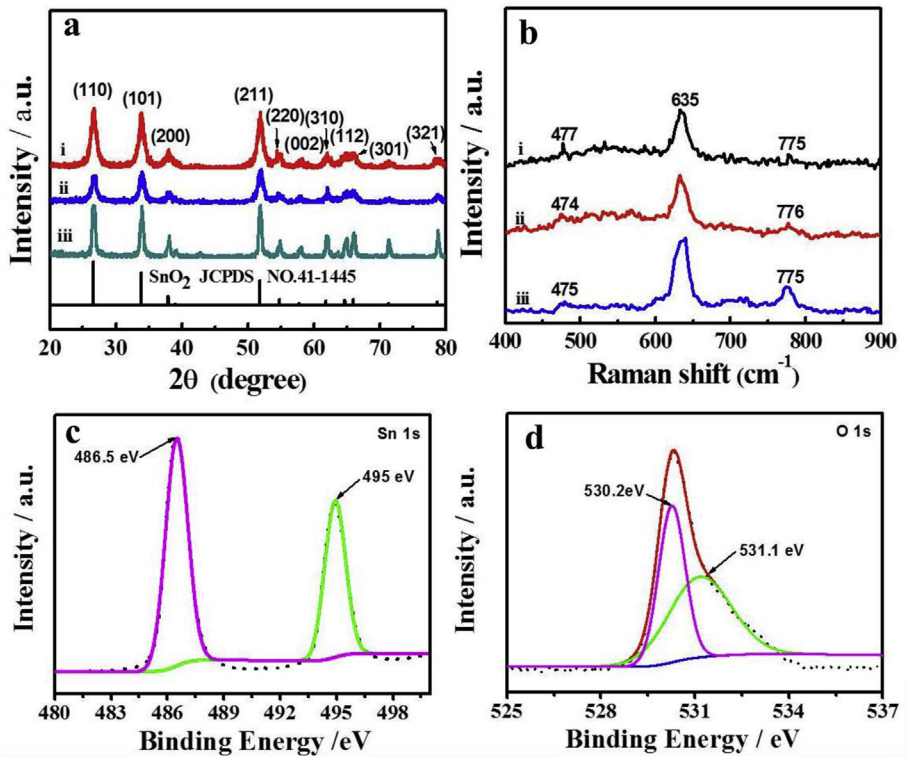

Fig. 1 – (a) XRD patterns of (i) SnO_2–I, (ii) SnO_2-II, (iii) SnO_2-III; (b) Raman spectra of (i) SnO_2–I, (ii) SnO_2-II, (iii) SnO_2-III at room temperature; Sn 3d (c) and O1s (d) XPS spectra of the SnO_2–I.

Please cite this article in press as: Song H, et al., Controllable lithium storage performance of tin oxide anodes with various particle sizes, International Journal of Hydrogen Energy (2015), http://dx.doi.org/10.1016/j.ijhydene.2015.03.168

The working electrodes were prepared by slurry-casting on 25 um-thick Cu foils served as current collectors. The slurry contained 80 wt% anode material, 10 wt% carbon black and 10 wt% polyvinylidene fluoride binder in the N-methyl-pyrrolidinone (NMP) solvent. The obtained electrodes were dried in a vacuum at 80 °C overnight. The SnO_2 electrodes and the lithium foils were used as the working electrodes and the counter electrodes, respectively. The electrolyte was composed of 1 M $LiPF_6$ salt dissolved in a 1:1 mass ratio of ethylene carbonate (EC) and dimethyl carbonate (DMC). The electrochemical performance of the anode materials was studied using 2032 type coin cells. The coin cells were assembled in an argon-filled glove box (both moisture and oxygen level are less than 1.0 ppm). The assembled cells were aged for 12 h before the electrochemical performance measurements. Charge-discharge characteristics were galvanostatically tested between 0.01 and 3.0 V (vs. Li/Li^+) at room temperature using LANHE CT2001A. Cyclic voltammograms (the scan rate of 0.1 mV s^{-1} and a potential range of 0.01–3.0 V (vs. Li/Li^+)) and electrochemical impedance spectra (the frequency was varied from 0.1 MHz to 0.01 Hz with potential amplitude of 5 mV) were performed on Princeton Applied Research VersaSTAT 4.

Results and discussion

The powder X-ray diffraction was performed to examine the sample phases with various particle sizes. Fig. 1a shows the XRD patterns of the SnO_2 nanoparticles with three particle sizes. It can be seen that all XRD patterns samples well match the pure phase of SnO_2 (JCPDS No. 41–1445). But some difference was found that SnO_2–I shows broader peaks in comparison to SnO_2-II and SnO_2-III, which indicated that this sample exhibits the smallest particle size [13]. Based on the Scherrer's equation:

$$D = K^*\lambda/B^*\cos\theta (k = 0.89)$$

One can calculate that the particle sizes of SnO_2–I, SnO_2-II, and SnO_2-III are about 11.7 nm, 26.8 nm, and 78.4 nm, respectively. Derived from the group theory of rutile structure vibration mode, G (Gibbs free energy) = $A_{1g} + A_{2g} + A_{2u} + B_{1g} + B_{2g} + 2B_u + E_g + 3E_u$. In the equation, A_{1g}, B_{1g}, B_{2g} and E_g are Raman active. A_{2u} and E_u are related to transverse optical vibration mode (TO) and longitudinal optical

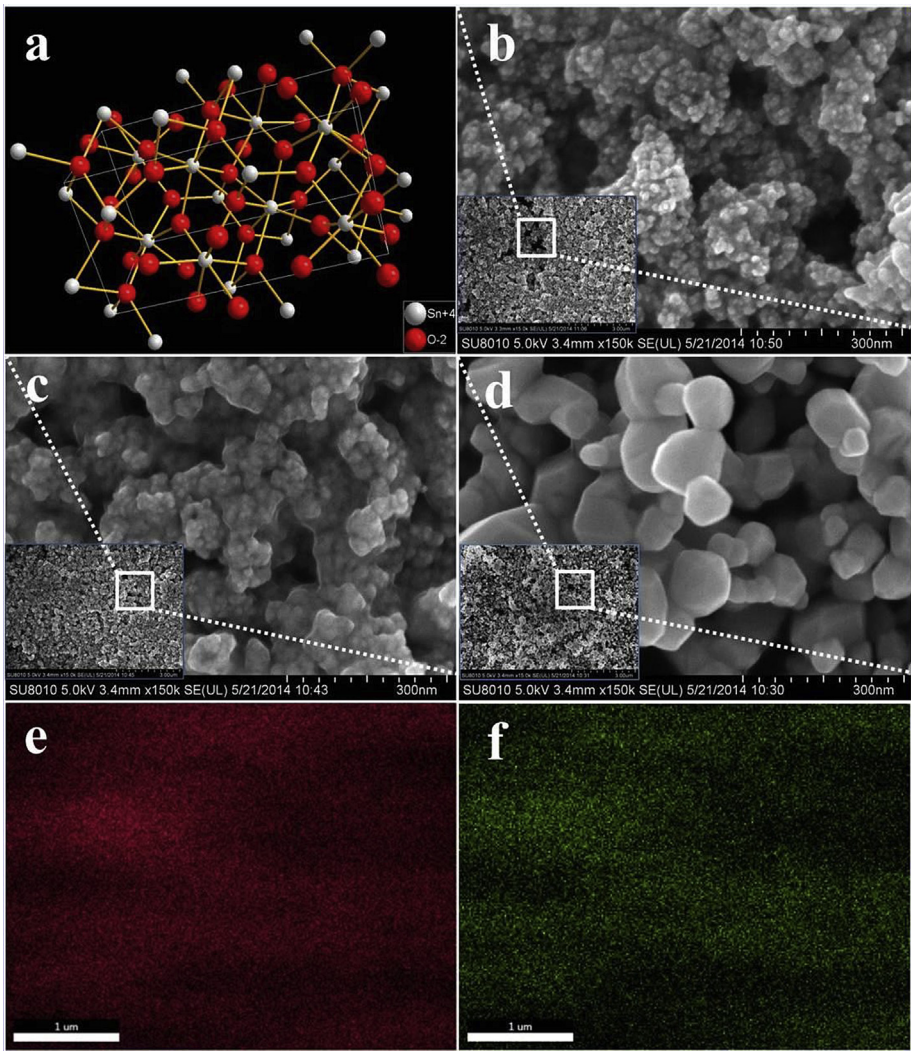

Fig. 2 – (a) Typical SnO_2 structural model; SEM images of (b) SnO_2–I, (c) SnO_2-II, (d) SnO_2-III at different magnification; Mapping of (e) Sn element and (f) O element of SnO_2–I.

Please cite this article in press as: Song H, et al., Controllable lithium storage performance of tin oxide anodes with various particle sizes, International Journal of Hydrogen Energy (2015), http://dx.doi.org/10.1016/j.ijhydene.2015.03.168

vibration modes (IO), respectively [12]. Fig. 1b shows room-temperature Raman spectra of the SnO_2 nanomaterials. The fundamental Raman scattering peaks of SnO_2–I were observed at 477, 635, and 775 cm^{-1}, which correspond to the E_g, A_{1g}, and B_{2g} vibration modes, respectively [13]. The similar vibration modes were discovered in the other two samples. However, the peak intensity of the B_{2g} vibration mode reduced as order: SnO_2-III > SnO_2-II > SnO_2–I. It is well known that the Raman spectra are highly dependent on excitations from the resonance behavior as well as structural factors or the wavelength of laser [14]. Thus, it is believed that the various vibration mode of SnO_2 results from the different particle size [13].

Fig. 1c shows the Sn 3d5/2 and Sn 3d3/2 peaks located at 486.5 eV and 495 eV in the fine spectrum of Sn 3d, which also confirm the SnO_2 formation [15]. The gap between the two peaks is 8.5 eV, close to Sn (3d) peak in the standard SnO_2 XPS spectrum. The O (1s) spectrum (Fig. 1d) shows a maximum close to 530 eV, which can be attributed to the existence of O^{2-} species in the SnO_2. The Sn 3d spectrum and the O 1s spectrum can prove the presence of SnO_2 in the obtained product. The peak position located at 530.2 eV is the equivalent of lattice oxygen in the SnO_2. Another O peak at 531.1 eV confirmed the surface oxygen of the nanoscaled SnO_2.

Cassiterite belongs to space group $P4_2/mnm$ with a = 4.738 Å and c = 3.187 Å [16–20]. XRD and Raman results indicate that SnO_2 nanoparticles reveal the main characteristics of rutile structure, as shown in Fig. 2a. In this study, three SnO_2 nanoparticles with different size were compared for lithium ion batteries, and the particle sizes of SnO_2–I, SnO_2-II, and SnO_2-III are tested by SEM in Fig. 2b–d. It can be observed that the particle sizes of SnO_2–I, SnO_2-II, and SnO_2-III are 15 nm, 30 nm and 70 nm, respectively. The Sn and oxygen element mappings of the anode materials are shown in Fig. 2e and f and Fig. S3 and 4, confirm the uniform distribution of Sn and O in the anode material.

Transmission electron microscopy (TEM) observations were employed to further characterize the SnO_2–I morphology. Fig. 3a displays the typical TEM micrographs of the SnO_2–I. The as-synthesized SnO_2 sample shows average particle size of 15 nm, which is in good agreement with the SEM observation. The EDX spectrum of the SnO_2–I is embedded in Fig. 3a. The EDX spectrum confirms that the product is composed of Sn and O elements. Fig. S1 a, b show the EDX spectra of the other two samples, respectively. No other elements were detected, which indicates that as-prepared SnO_2 exhibits high purity. As marked in the HRTEM micrographs (Fig. 3b), interplanar spacing of 0.333 and 0.264 nm can be clearly observed, which corresponds to the (110) and (101) planes of rutile SnO_2, respectively. The ring-like selected-area electron diffraction (SAED) pattern in Fig. 3c indicates that the nanoparticles exhibit a polycrystalline structure, and the diffraction rings from inside to outside can be indexed to the (110), (101), (211), and (220) planes of rutile SnO_2, respectively. Fig. 3d is Fourier transform of Fig. 3b, and these indexed patterns are consistent with the XRD reflections.

Cyclic voltammetry was carried out in the voltage range of 0.1–3.0 V (vs. Li^+/Li) at a scan rate of 0.1 mV s^{-1} to identify the electrochemical reactions of the anode materials with lithium, as presented in Fig. 4a–c. These CV profiles show a typical SnO_2 electrochemical behavior with lithium. The cathodic sweep process exhibits two characteristic peaks. One peak is located at 0.9 V originating from the decomposition of SnO_2 into Sn combined with the formation of Li_2O: $SnO_2 + 4Li^+ + 4e^- \rightarrow Sn + 2Li_2O$, and solid electrolyte

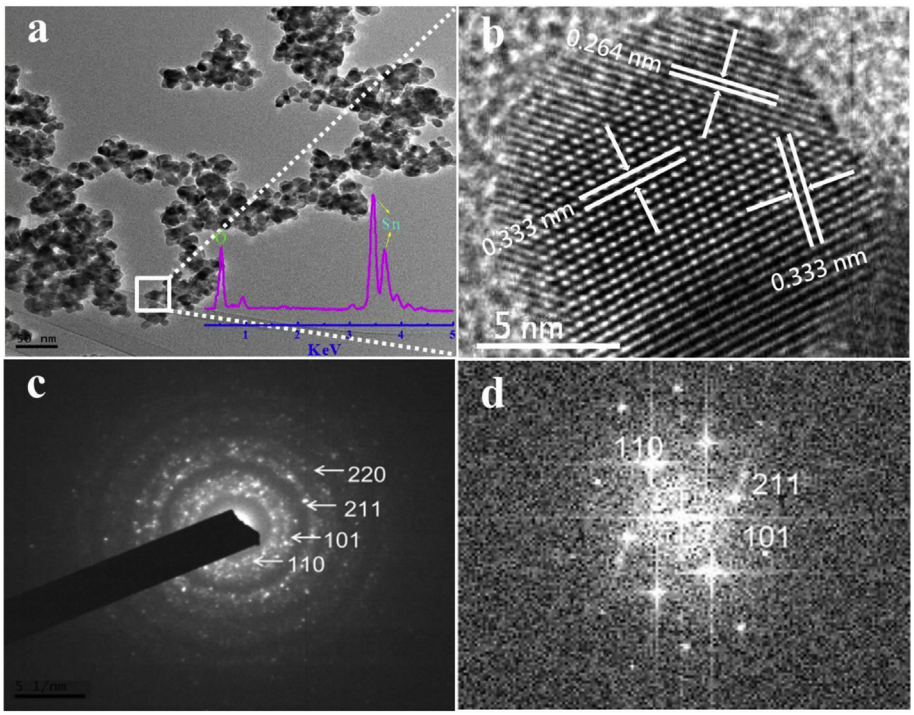

Fig. 3 – (a) TEM observation and EDS spectrum of SnO_2–I; (b) The lattice spacing and (c) selected-area diffraction (SAED) patterns of SnO_2–I; (d) Fourier transform of Fig. 3b.

Please cite this article in press as: Song H, et al., Controllable lithium storage performance of tin oxide anodes with various particle sizes, International Journal of Hydrogen Energy (2015), http://dx.doi.org/10.1016/j.ijhydene.2015.03.168

interphase (SEI) formation [11]. The other characteristic peak is positioned at 0.2 V, which results from alloying of Sn with Li as described: $Sn + xLi^+ + xe^- \rightarrow Li_xSn$ ($0 \le x \le 4.4$) [21–23]. The oxidation process also shows two peaks. In the anodic sweep process, one peak at 0.5 V represents the dealloying of Li_xSn as described: $Li_xSn \rightarrow Sn + xLi^+ + xe^-$ ($0 \le x \le 4.4$) [24,25]. It was confirmed that the SnO_2 size does not show an obvious effect on the redox reactions. However, the reduction and oxidation areas show some difference in various cycles. With the increase of particle size, this phenomenon is more obvious, which indicates that SnO_2 with decreased particle size exhibits better electrochemical stability.

Fig. 4d–f show the typical voltage profiles of three SnO_2 nanoparticles. It is observed that there exists a large difference between discharge and charge capacities with an irreversible capacity loss in the first cycle. The first discharge capacities of SnO_2–I, SnO_2-II, and SnO_2-III are 1800, 1250, and 1520 mAh g^{-1}, respectively. It is worth to note that the initial irreversible capacities of the SnO_2–I (900 mAh g^{-1}), the SnO_2-II (620 mAh g^{-1}), and the SnO_2-III (690 mAh g^{-1}) are related to SEI formation and irreversible reaction of $SnO_2 + 4Li^+ + 4e^- \rightarrow Sn + 2Li_2O$ [26–31]. In the first discharge step, the initial small plateau in the potential range of 1.5 to 0.8 V is observed for three materials, corresponding to the irreversible reduction and SEI formation, similar to the SnO_2 results previously reported [32–39]. However, this plateau almost disappears in the following cycles.

Fig. 5a and b compare the discharge capacity and coulombic efficiency versus cycle numbers of SnO_2–I, SnO_2-II and SnO_2-III. The discharge capacities of SnO_2–I, SnO_2-II, and SnO_2-III after 30 cycles are about 460, 280 and 180 mAh g^{-1}, respectively. Compared with the second discharge capacity, the capacity retention of SnO_2–I, SnO_2-II, and SnO_2-III is around 58.2%, 40.7% and 21.9%, respectively. By contrast, the enhanced lithium storage performance of SnO_2–I can be attributed to the reduction of particle size, which can alleviate the volume variation of SnO_2 [36]. It is well known that the main hindrance against commercialization of Sn based anode materials in LIBs is the large volume variation during charge/discharge processes which leads to poor cyclability [16]. The nature of fast attenuation capacity is due to volume change, which causes a so-called pulverization problem hindering the electrical connection in the electrode. It was reported that SnO_2 shows increased performance with the decrease of the anode nanoparticle size [40]. Our study confirms this important point. The initial coulombic efficiency of the three types SnO_2 electrodes were around 50%, which is due to the SEI layer formation of generated by an irreversible insertion/desertion of Li^+ into the host structures and the irreversible reaction of SnO_2 with lithium [41]. The coulombic efficiencies of all

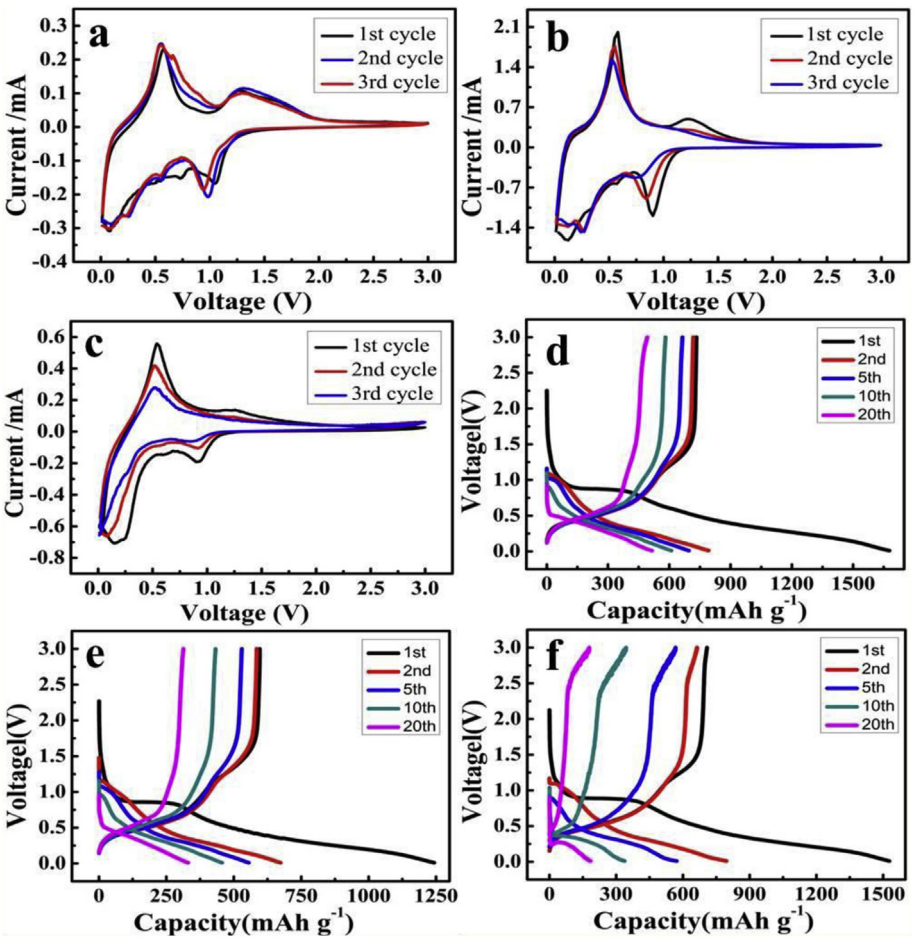

Fig. 4 – CV curves of (a) SnO_2–I, (b) SnO_2-II and (c) SnO_2-III at a scan rate of 0.1 mV s^{-1} in the voltage of 0.01–3.0 V; Charge and discharge curves of (d) SnO_2–I, (e) SnO_2-II and (f) SnO_2-III obtained in the 1st, 2nd, 5th, 10th, 20th cycles.

Please cite this article in press as: Song H, et al., Controllable lithium storage performance of tin oxide anodes with various particle sizes, International Journal of Hydrogen Energy (2015), http://dx.doi.org/10.1016/j.ijhydene.2015.03.168

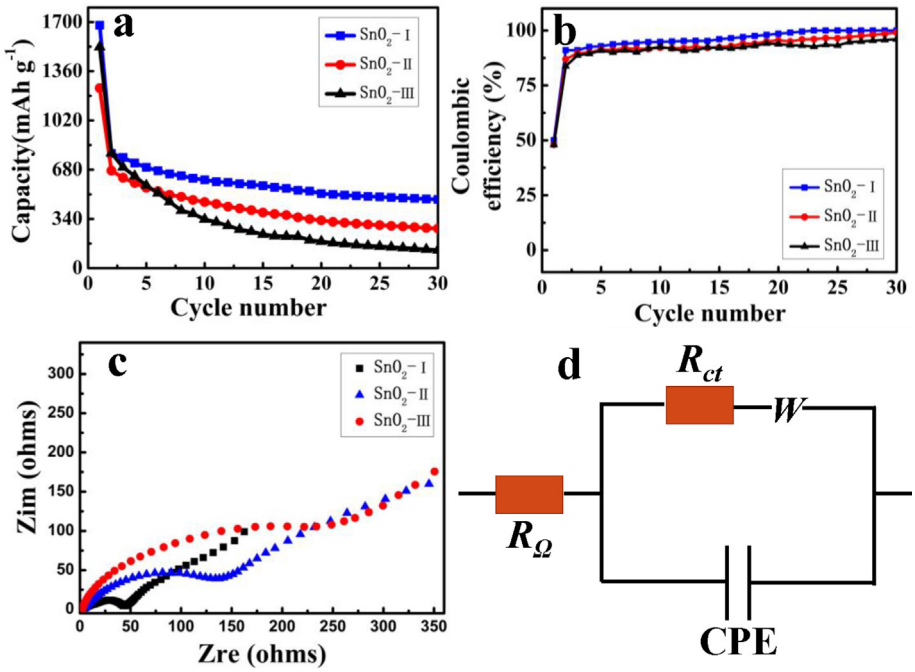

Fig. 5 – (a) Cycling performance and (b) Coulombic efficiency of SnO_2–I, SnO_2-II and SnO_2-III at the current density of 100 mA g^{-1}; (c) Electrochemical impedance spectroscopy of SnO_2–I, SnO_2-II and SnO_2-III; (d) The equivalent circuit diagram for fitting impedance spectra in Fig. 5c.

samples reach more than 90% after two cycles. In addition, the relevant coulombic efficiency of SnO_2–I maintains around 100% after several cycles, indicating the good electrochemical reversibility. The results may be related to higher crystal degree and larger specific surface area [40].

Electrochemical impedance spectroscopy (EIS) was conducted to determine the Li^+ transfer behavior in the SnO_2–I, SnO_2-II and SnO_2-III, as shown in Fig. 5c. It is well known that the high frequency semicircle is related to the charge-transfer resistance at the interface between the electrolyte and the electrode material. The inclined line corresponds to the Li^+ diffusion into the electrode material [28]. The semicircle diameters of SnO_2–I are smaller than that of the other two samples, indicating that reduction of particle size increases electron and lithium ion transfer rates [38]. The equivalent circuit diagram in Fig. 5d was employed to simulate the EIS curves. It was reported that the EIS of the porous powder electrodes tend to deviate from the ideal smooth electrodes due to the dispersion effect [32]. Thus, the introduction of constant-phase element (CPE) in the equivalent circuit of Fig. 5d fits the influence of dispersion effect on the impedance spectrum [33]. It was found that the charge transfer resistance (R_{ct}) of SnO_2–I, SnO_2-II, and SnO_2-III is 104.1, 130.4, and 178.2 Ω, respectively. Clearly, SnO_2 with smaller particle size facilitates the electrochemical reaction of the anode with lithium, which results in the decreased R_{ct} value. The quick charge transfer in SnO_2 leads to their superior electrochemical performances. Therefore, SnO_2–I exhibits the best performance among three anode materials.

The schematic illustration of morphological evolution of as-prepared SnO_2 nanoparticles is shown in Scheme 1. The SnO_2 anode with the biggest particle size (say SnO_2-III) suffers from the huge volume change, resulting in the serious pulverization upon cycling (Scheme 1a), which is the main reason why SnO_2-III exhibits the poorest performance in Fig. 5a. When the particle size of SnO_2 decreases, the resultant absolute volume change decreases as well. It shows some improvement of the anode pulverization in Scheme 1b. Furthermore, the particle size of the anode decreases down to 15 nm (say SnO_2–I), and in Scheme 1c, the pulverization improvement shows the best positive effect originating from the smallest volume change among these three anode materials. Therefore, as shown Fig. 5a, SnO_2–I with the smallest particle size reveals the best anode performance for lithium ion batteries.

Conclusions

In summary, a facile reflux method was developed to synthesize SnO_2–I nanoparticles with smaller particle size than SnO_2-II synthesized via the hydrothermal approach. XRD, SEM and HRTEM results revealed that the particle sizes of SnO_2–I, SnO_2-II, and SnO_2-III are around 10 nm, 30 nm and 70 nm, respectively. These three SnO_2 nanomaterials were studied as the anodes for lithium ion batteries. The obtained electrochemical results confirm that SnO_2–I exhibits better cycling performance than the other two materials. Moreover, the coulombic efficiency of SnO_2–I maintains close to 100% after several cycles, which is higher than those of SnO_2-II and SnO_2-III. It was found that the increased performance of SnO_2–I results from smaller particle size with lower absolute volume change during charge/discharge processes. Therefore, the significant impact of SnO_2 particle size on battery performance was clearly demonstrated, which opens a potential

Please cite this article in press as: Song H, et al., Controllable lithium storage performance of tin oxide anodes with various particle sizes, International Journal of Hydrogen Energy (2015), http://dx.doi.org/10.1016/j.ijhydene.2015.03.168

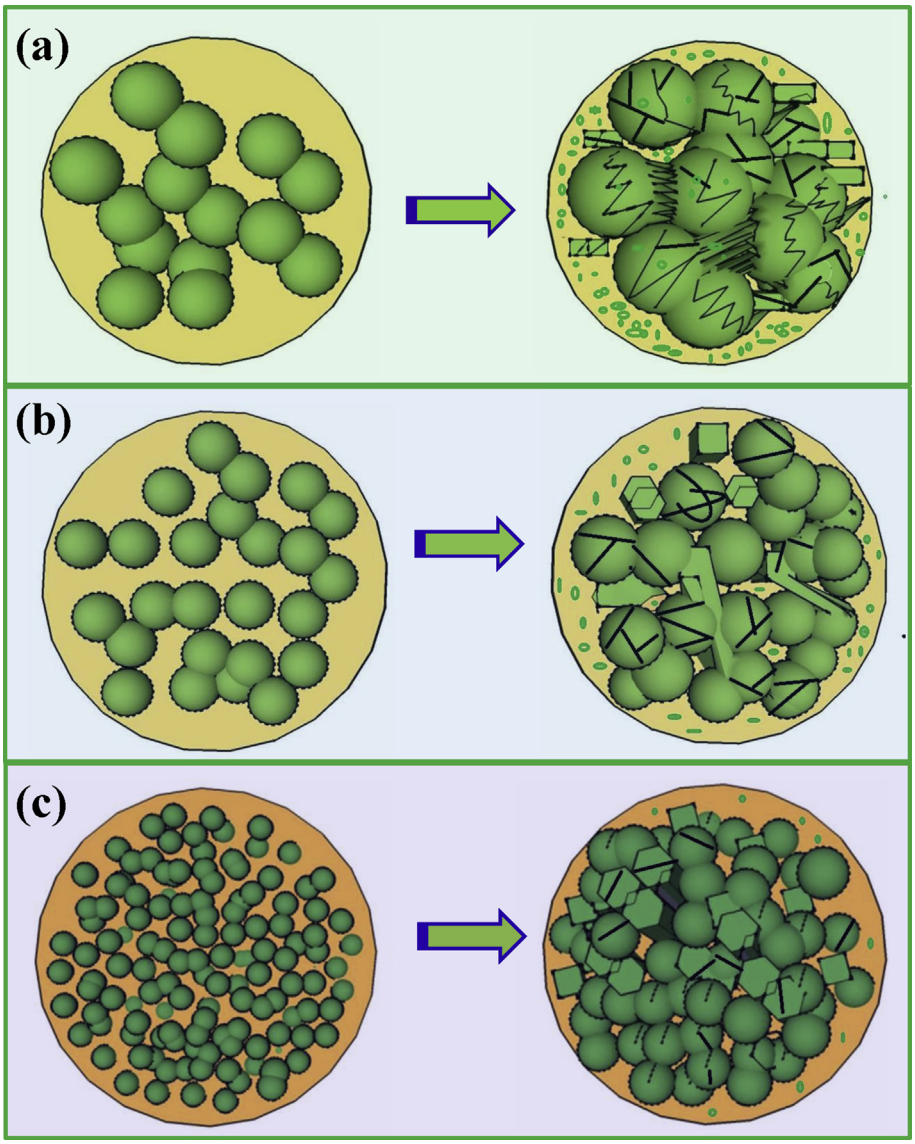

Scheme 1 – The morphological evolution of (a) SnO_2–I, (b) SnO_2-II and (c) SnO_2-III before and after cycles (Left figures: before cycles; Right figures: after cycles).

door to further increase SnO_2 performance for possible commercialization in high performance lithium ion batteries.

Acknowledgements

This research was supported by Key Project of Tianjin Municipal Natural Science Foundation of China (13JCZDJC33900 and 14JCZDJC32200), Key Laboratory of Functional Inorganic Material Chemistry (Heilongjiang University), Ministry of Education, LPMT, CAEP (KF14006 and ZZ13007), Project 2013A030214 supported by CAEP, Science & Technology Department of Sichuan Province (2013GZX0145-3), Academic Innovation Funding of Tianjin Normal University (52XC1404), Scientific Research Foundation of Tianjin Normal University (5RL131), Training Plan of Leader Talent of University in Tianjin, Scientific Research Foundation for Returned Overseas Chinese Scholars of State Education Ministry, and the program of Thousand Youth Talents in Tianjin of China.

Appendix A. Supplementary data

Supplementary data related to this article can be found at http://dx.doi.org/10.1016/j.ijhydene.2015.03.168

REFERENCES

[1] Simonin L, Lafont U, Kelder EM. SnSb micron-sized particles for Li-ion batteries. J Power Sources 2008;180:859–63.
[2] Li Y, Lv X, Lu J, Li J. Preparation of SnO_2-nanocrystal/graphene-nanosheets composites and their lithium storage ability. J Phys Chem C 2010;114:21770–4.

[3] Huggins RA. Lithium alloy negative electrodes formed from convertible oxides. Solid State Ionics 1998;113–115:57–67.
[4] Wang J, Raistrick ID, Huggins RA. Behavior of some binary Lithium alloys as negative electrodes in organic solvent-based electrolytes. J Electrochem Soc 1986;133:457–60.
[5] Winter M, Besenhard JO. Electrochemical lithiation of tin and tin-based intermetallics and composites. Electrochim Acta 1999;45:31–50.
[6] Besenhard JO, Yang J, Winter M. Will advanced lithium-alloy anodes have a chance in lithium-ion batteries? J Power Sources 1997;68:87–90.
[7] Wang Y, Lee JY. Molten salt synthesis of tin oxide nanorods: morphological and electrochemical features. J Phys Chem B 2004;108:17832–7.
[8] Beaulieu LY, Eberman KW, Turner RL, Krause LJ, Dahn JR. Colossal reversible volume changes in lithium alloys. Electrochem Solid-State Lett 2001;4:A137–40.
[9] Kilibarda G, Szabó DV, Schlabach S, Winkler V, Bruns M, Hanemann T. Investigation of the degradation of SnO_2 electrodes for use in Li-ion cells. J Power Sources 2013;233:139–47.
[10] Zhu J, Zhang G, Yu X, Li Q, Lu B, Xu Z. Graphene double protection strategy to improve the SnO_2 electrode performance anodes for lithium-ion batteries. Nano Energy 2014;3:80–7.
[11] Cheng M, Ye Y, Chiu T, Pan C, Hwang B. Size effect of nickel oxide for lithium ion battery anode. J Power Sources 2014;253:27–34.
[12] Sathish M, Mitani S, Tomai T, Unemoto A, Honma I. Nanocrystalline tin compounds/graphene nanocomposite electrodes as anode for lithium-ion battery. J Solid State Electrochem 2012;16:1767–74.
[13] Li XF, Liu J, Meng X, Tang Y, Banis MN, Yang J, et al. Significant impact on cathode performance of lithium-ion batteries by precisely controlled metal oxide nanocoatings via atomic layer deposition. J Power Sources 2014;247:57–69.
[14] Gao T, Fjellvåg H, Norby P. Structural and morphological evolution of β-MnO_2 nanorods during hydrothermal synthesis. Nanotechnology 2009;20:055610.
[15] Park M, Kang Y, Wang G, Dou S, Liu H. The effect of morphological modification on the electrochemical properties of SnO_2 nanomaterials. Adv Funct Mater 2008;18:455–61.
[16] Guo ZP, Wang JZ, Liu HK, Dou SX. Study of silicon/polypyrrole composite as anode materials for Li-ion batteries. J Power Sources 2005;146:448–51.
[17] Yang Z, Du G, Feng C, Li S, Chen Z, Zhang P, et al. Synthesis of uniform polycrystalline tin dioxide nanofibers and electrochemical application in lithium-ion batteries. Electrochim Acta 2010;55:5485–91.
[18] Zhang M, Lei D, Yu X, Chen L, Li Q, Wang Y, et al. Graphene oxide oxidizes stannous ions to synthesize tin sulfide-graphene nanocomposites with small crystal size for high performance lithium ion batteries. J Mater Chem 2012;22:23091–7.
[19] Kil K, Lee M, Kim G, Cho C, Kim K, Kim G, et al. Enhanced electrochemical properties of $LiFePO_4$ electrodes with carboxylated poly(vinyl difluoride) in lithium-ion batteries: experimental and theoretical analysis. J Phys Chem C 2011;115:16242–6.
[20] Xia H, Tang S, Lu L. Properties of amorphous Si thin film anodes prepared by pulsed laser deposition. Mater Res Bull 2007;42:1301–9.
[21] Chen W, Ghosh D, Chen S. Large-scale electrochemical synthesis of SnO_2 nanoparticles. J Mater Sci 2008;43:5291–9.
[22] Lou XW, Wang Y, Yuan C, Lee JY, Archer LA. Template-free synthesis of SnO_2 hollow nanostructures with high lithium storage capacity. Adv Mater 2006;18:2325–9.
[23] Li Y, Guo Y, Tan R, Cui P, Li Y, Song W. Selective synthesis of SnO_2 hollow microspheres and nano-sheets via a hydrothermal route. Chinese Sci Bull 2010;55:581–7.
[24] Kösea H, Aydina AO, Akbulutb H. The effect of temperature on grain size of SnO_2 nanoparticles synthesized by sol-gel method. Acta Phys Pol A 2014;125:345–7.
[25] Li XF, Dhanabalan A, Wang C. Three-dimensional porous core-shell Sn@Carbon composite anodes for high-performance lithium-ion battery applications. Adv Energy Mater 2012;2:238–44.
[26] Connor PA, Irvine JTS. Novel tin oxide spinel-based anodes for li-ion batteries. J Power Sources 2001;97–98:223–5.
[27] Kim C, Noh M, Choi M, Cho J, Park B. Critical size of a nano SnO_2 electrode for li-secondary battery. Chem Mater 2005;17:3297–301.
[28] Yang R, Gu Y, Li Y, Zheng J, Li X. Self-assembled 3-D flower-shaped SnO_2 nanostructures with improved electrochemical performance for lithium storage. Acta Mater 2010;58:866–74.
[29] Wu G, Li Z, Wu W, Wu M. Effects of calcination on the preparation of carbon-coated SnO_2/graphene as anode material for lithium-ion batteries. J Alloy Compd 2014;615:582–7.
[30] Liu H, Huang J, Li X, Liu J, Zhang Y, Du K. Flower-like SnO_2/graphene composite for high-capacity lithium storage. Appl Surf Sci 2012;258:4917–21.
[31] Yang X, Fan K, Zhu Y, Shen J, Jiang X, Zhao P, et al. Tailored graphene-encapsulated mesoporous Co_3O_4 composite microspheres for high-performance lithium ion batteries. J Mater Chem 2012;22:17278–83.
[32] Li XF, Wang CL, Mater J. Engineering nanostructured anodes via electrostatic spray deposition for high performance lithium ion battery application. J Mater Chem A 2013;1:165–82.
[33] Li XF, Meng XB, Liu J, Geng DS, Zhang Y, Banis MN, et al. Tin oxide with controlled morphology and crystallinity by atomic layer deposition onto graphene nanosheets for enhanced lithium storage. Adv Funct Mater 2012;22:1647–54.
[34] Li XF, Zhong Y, Cai M, Balogh MP, Wang D, Zhang Y, et al. Tin-alloy heterostructures encapsulated in amorphous carbon nanotubes as hybrid anodes in rechargeable lithium ion batteries. Electrochim Acta 2013;89:387–93.
[35] Zhao Y, Li XF, Yan B, Li DJ, Lawes S, Sun XL. Significant impact of 2D grapheme nanosheets on large volume change tin-based anodes in lithium-ion batteries: a review. J Power Sources 2015;274:869–84.
[36] Winter M, Besenhard JO, Spahr ME, Novak P. Insertion electrode materials for rechargeable lithium batteries. Adv Mater 1998;10:725–63.
[37] Claye AS, Fischer JE, Huffman CB, Rinzler AG, Smalley RE. Solid-state electrochemistry of the li single wall carbon nanotube system. J Electrochem Soc 2000;147:2845–52.
[38] Wu GT, Wang CS, Zhang XB, Yang HS, Qi ZF, He PM, et al. Structure and lithium insertion properties of carbon nanotubes. J Electrochem Soc 1999;146:1696–701.
[39] Song HW, Li N, Cui H, Wang CX. Enhanced capability and cyclability of SnO_2-grapheme oxide hybrid anode by firmly anchored SnO_2 quantum dots. J Mater Chem A 2013;1:7558–62.
[40] Wu G, Wu M, Wang D, Yin L, Ye J, Deng S, et al. A facile method for in-situ synthesis of SnO_2/graphene as a high performance anode material for lithium-ion batteries,. Appl Surf Sci 2014;315:400–6.
[41] Song HJ, Zhang LC, He CL, Qu Y, Tian YF, Lv Y. Graphene sheets decorated with SnO_2 nanoparticles: in situ synthesis and highly efficient materials for cataluminescence gas sensors. J Mater Chem 2011;21:5972–7.

Please cite this article in press as: Song H, et al., Controllable lithium storage performance of tin oxide anodes with various particle sizes, International Journal of Hydrogen Energy (2015), http://dx.doi.org/10.1016/j.ijhydene.2015.03.168